Powder Technology 404 (2022) 117418

Contents lists available at ScienceDirect

Powder Technology

journal homepage: www.elsevier.com/locate/powtec

Utilising micron scale 3D printed morphologies for particle adhesion reduction

Georgina E. Marsh [a,*,1], Matt J. Bunker [d], Morgan R. Alexander [b], Ricky D. Wildman [c], Mark Nicholas [e], Clive J. Roberts [b]

[a] School of Pharmacy, University of Nottingham Malaysia, Semenyih, Malaysia
[b] School of Pharmacy, University of Nottingham, Nottingham, UK
[c] Department of Chemical and Environmental Engineering, University of Nottingham, Nottingham, UK
[d] AstraZeneca Oral Product Development, PT&D, Operations, AstraZeneca, Macclesfield, UK
[e] AstraZeneca R&D, Mölndal, Sweden

ARTICLE INFO

Article history:
Received 9 March 2022
Received in revised form 18 April 2022
Accepted 19 April 2022
Available online 28 April 2022

Keywords:
Two photon polymerisation
AFM
Particle-surface adhesion
Surface roughness

ABSTRACT

In the pharmaceutical industry, the ability to improve the understanding of the effect of surface roughness on interparticulate interactions is critical. Dry powder inhalers often possess poor efficiency, as the powder formulations are inherently adhesive and cohesive due to their size. The complex interplay of factors that affect interparticulate interactions, means it has been difficult to isolate the effect of surface morphology. Using two photon polymerisation, this study shows the fabrication of bespoke sub-micron geometric structures, with a consistent surface chemistry. These are used to investigate the effect of surface morphologies on particle adhesion by utilising AFM force-volume mapping, to model spheres and carrier particles. This demonstrates the significant effect varying surface morphology can have on particle-surface adhesion. This approach allows for the first time an in-depth examination of the local variation effect of surface features on particle adhesion and may facilitate the design and optimisation of powder processes.

1. Introduction

Understanding of particulate adhesion and cohesion is a critical aspect of the operation and process efficiency of several industries. For instance, adhesion of fine particles to electronics in the semiconductor industry [1], and to surfaces in nuclear fusion facilities [2] as well as soiling of solar panels, reduces performance [3]. In the pharmaceutical industry, interparticulate interactions are particularly crucial, due to the use of powders in many formulations and manufacturing steps, including; tablet punch sticking [4], powder flow for tablet die filling [5], and inhaler actuation [6].

Focusing on pulmonary drug delivery specifically, for drug particles to exert a pharmacological effect on their target, particles must possess an aerodynamic diameter less than 5 μm [7]. Due to this size restriction particles are cohesive [8] and adhesive [9], due to their high surface to volume ratio. With adhering of particles to the device walls [10,11] and failure to de-aggregate during aerosolization, dry powder inhalers (DPIs) often struggle to produce a fine particle fraction efficiency above 15% [12], with device powder retention reported as high as 60% [13].

Therefore, gaining new fundamental insight to evaluate and reduce particle adhesion is essential in improving device performance. It is known that there is a combination of highly inter-related factors which affect interparticulate interactions in a complex manner including; surface roughness, surface chemistry, particle size/ shape and particle mechanical properties (e.g. elastic modulus) [14,15]. The capability to elucidate in detail the particle adhesion effect of systematically altered surface morphology, in isolation of other factors affecting particle adhesion would greatly assist in gaining such fundamental insight. Surface roughness has a particularly important role in the extent of particle-surface adhesion [1,16]. For small particles, the primary adhesive force results from van der Waal interactions, which mainly operate over very short distances. Therefore, the presence of small-scale roughness (less than the dimensions of the particles involved) can reduce the effective particle-surface contact area, resulting in a reduction of adhesion. As the scale of the roughness increases however, a phenomenon called mechanical interlocking can ensue with the entrapment of a

Abbreviations: AFM, Atomic Force Microscopy; DPIs, Dry Powder Inhalers; TPP, Two Photon Polymerisation; CPM, Colloidal Probe Microscopy.

* Corresponding author.
E-mail address: georgina.marsh@nottingham.edu.my (G.E. Marsh).
[1] Present address at: School of Pharmacy, University of Nottingham Malaysia, Malaysia, 43500 Semenyih.

https://doi.org/10.1016/j.powtec.2022.117418

particle or asperity in the surface roughness, dramatically increasing particle-surface adhesion [17].

Previous attempts to evaluate the impact of varying surface morphologies, often use destructive techniques to generate different degrees of roughness [18] with no effective control over the morphologies generated, and often produce a change in surface energy and hence a convolution of factors that influence adhesion.

This paper aims to demonstrate the production of well-defined micron scale morphologies with a consistent and controllable surface chemistry by combining two photon polymerisation 3D printing (geometry) and a plasma polymerisation coating approach (chemistry). The resultant surface morphologies can then be altered in a controllable fashion and hence used to evaluate trends in particle adhesion, without changing other factors.

Two photon polymerisation (TPP) is a high- resolution 3D printing technique, similar to stereolithography, based upon localised curing of a photoinitiated polymer resin. The principle of multi-photon absorption [19] is used, cross-linking the photoresist by focusing the beam of a femto-second infra-red laser [20]. By spatial and temporal compression, a sufficient photon density is achieved overcoming the threshold for two photon absorption. As the polymer resin molecules cannot be excited by a single infra-red photon, this effect is extremely localised in all directions allowing a high degree of design control and 3D structure capability [21,22]. Therefore, TPP can achieve a sub-diffraction limit lateral resolution of 120 nm or better [23], demonstrating at least an order of magnitude improvement in spatial resolution over other current state of the art 3D printers. Both nano-and micro-scale roughness can therefore be produced and systematically varied.

Particle adhesion measurements can be obtained by a variety of techniques. Many, like the centrifuge [24,25], drop [26] or vibration technique [27], rely on ensemble bulk powder adhesion measurements, producing a distribution based on the varying numbers of particles detached for a given force. Although often useful for evaluating a general ranking of particle-surface interactions, it is difficult to evaluate how individual local surface features are affecting the interaction with these approaches.

Atomic force microscopy (AFM), has been widely used for a range of biological and pharmaceutical applications, due to its high degree of sensitivity to local surface interactions and topographical resolution under ambient or liquid conditions [28]. AFM works by scanning a sharp probe across a surface and monitoring the deflection of the supporting force sensitive cantilever, utilising a laser reflected from the cantilever. This is normally conducted with a nanoscale sharp tip as the probe, however colloidal probe microscopy as used here, involves the attachment of a particle to a tipless AFM cantilever [29]. The cantilever, with particle attached, is lowered until particle contact with the surface is detected, on removal, the particle will adhere to the surface resulting in a deflection of the cantilever being recorded [30]. As the probe continues to rise, adhesive force will eventually be exceeded and the probe (particle) will snap off the surface returning to its equilibrium position [31]. By collection of a range, or map, of such force-curves over a surface, topographical imaging and particle-surface interactions can be mapped [32,33]. By evaluating the force required to pull the particle away from the surface, the force of adhesion can be calculated, as well as other material properties, such as elasticity and hardness [34].

In this study we use 3D printing to produce well defined surface topographies and demonstrate the ability to decouple the effects of surface energy in powder interactions, allowing greater insight into fundamental DPI formulation and device development.

2. Materials and methods

All photoresists and solvents were used as sourced. The UV curable photoresist IP-L 780 was obtained from Nanoscribe GmbH, Germany. All solvents were obtained from Sigma- Aldrich. All AFM probes were purchased from Bruker (Cambridge, UK).

2.1. Two photon polymerisation

Well defined geometric designs were created using the three-dimensional computer aided design software, Creo. These micron scale surface topographies were fabricated by a commercially available TPP printer (Photonic Professional GT, Nanoscribe GmbH) equipped with an inverted microscope (Zeiss) and a 63× immersion objective, numerical aperture = 1.3. 50 μm length ridges were polymerised, on a glass coverslip coated with the photoresist IP-L 780, using Piezo mode, with a laser power of 40 mW and power scaling of 0.6 using perfect shape quality, a path optimisation feature. The unexposed region of the resist was dissolved using two, thirty minute submerges of the glass coverslip in propylene glycol monomethyl ether acetate (PGMEA ≥99.5%) followed by a two minute isopropanol (≥99.5%) wash.

To modify the height, the original CAD file was altered to change the aspect ratio of the TPP ridges, to produce ridges of three differing design heights; 1 μm, 3 μm and 5 μm.

A pattern of ridges was then printed for each height, with varying spacing; 1 μm, 3 μm and 8 μm.

2.2. Fabricated structure analysis

A Zeta-20 Optical profilometer (Zeta Instruments, CA, USA) was used to capture 2D and 3D images of the structures, to evaluate ridge spacing, using 100 x magnification with 0.013 μm step size.

AFM Images were then captured to verify the ridge height, in quantitative nanomechanical mode using a Dimension ICON (Bruker, Cambridge, UK). Bruker RTESPA-300 Antimony doped Silicon tips were used with spring constants of around 40 N/m and resonant frequencies of 320 kHz. Gwyddion software (version 2.22) (Czech Metrology Institute, Brno) was used for image analysis. Images were tilt corrected before use.

2.3. Plasma polymerisation

Plasma polymerisation coating was used to produce a consistent surface chemistry and surface energy without significantly altering surface topography. Plasma polymerisation has been shown to deposit evenly producing a very low surface roughness [35].

The custom built reactor used for the application of plasma polymer on substrates has been described elsewhere [36], but briefly the setup consists of two circular electrodes with 12.5 cm spacing encased in a cylindrical reactor (35 cm high, 17 cm diameter) connected to a 13.56 MHz radio frequency power source (Coaxial Power System Ltd.) to initiate the plasma. ppHex was generated using a power of 50 W and an initial monomer pressure of 300 mTorr until a deposition of 40 nm was reached as measured by the in-built quartz crystal microbalance (Leica).

Successful polymerisation was verified using control coverslips, by Tof-SIMS (Supplementary Information, Fig. 2) and water contact angle measurements. The static contact angle for ppHex coated substrates was measured as 96° ± 4° (Supplementary Information, Fig. 1), which is consistent with the hydrophobicity of this coating and in line with previous literature [37].

2.4. Colloidal probe attachment

AFM silicon nitride tipless V-shaped cantilevers (MLCT-010 A), were selected and calibrated using the thermal tune method [38], with spring constants calculated as 0.58–0.83 N/m. The cantilevers were then modified with a colloidal probe of either a 10 μm or 5 μm polystyrene bead (Sigma-Aldrich, Dorset, UK) or a Respitose SV003 particle (DFE Pharma, Goch, Germany) (Fig. 1). A 5 μm spherical particle was chosen as a model, to represent an API, with the 10 μm highlighting differences due to particle size and the Respitose particle used as an exemplar respiratory carrier particle.

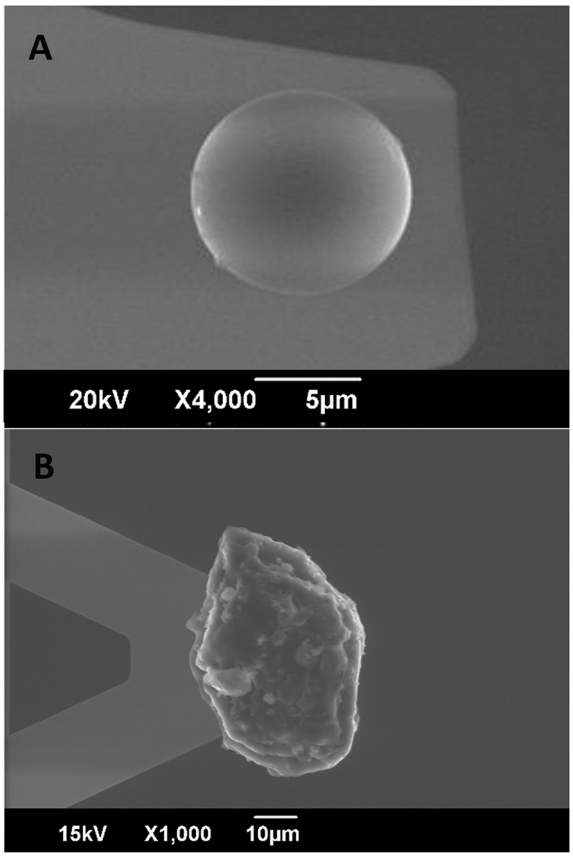

Fig. 1. SEM image of an example A) polystyrene 10 μm bead and B) Respitose SV003 particle used for colloidal probe microscopy.

Three of each type of colloidal probe were produced, attaching the particles using a MMAFM-2 Multimode AFM system (Digital Instruments, Santa Barbara, CA). Epoxy resin was dotted onto a silica wafer and spread into thin lines using a sacrificial probe. The tipless cantilever to be functionalised was then lowered until visual contact with the glue, and then withdrawn. This cantilever was then moved to an area with the powder and aligned with an isolated particle and then lowered manually onto the particle for attachment. The glue was left to dry for 24 h and then probe attachment was verified using low vacuum SEM images taken on a JEOL 6490 LV. This was achieved by placing the colloidal probe on a previously sputter coated AFM tip mount. Those particles centrally mounted and free from glue on the surface were used.

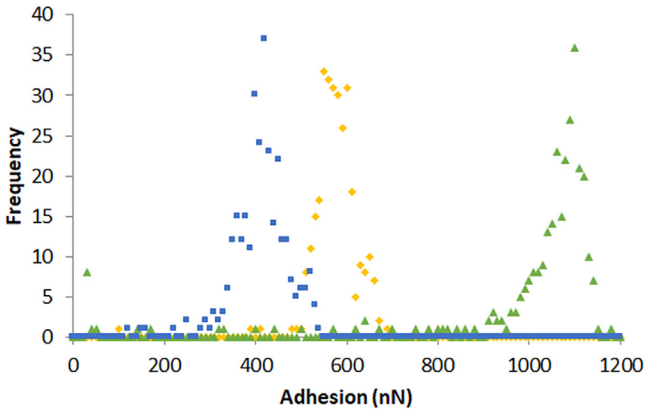

Fig. 3. A comparison of frequency curves of particle adhesion to the non-printed ppHex substrate for a polystyrene 10 μm bead (green Δ), a polystyrene 5 μm bead (yellow ◇) and a Respitose SV003 particle (blue □).

2.5. Adhesion measurements

All adhesion measurements were conducted using the auto ramp mode with a ramp rate of 0.93 Hz, on an Enviroscope AFM (BrukerNano), fitted with a Triton humidity controller, set to RH 10%. In order to convert the photodiode signal to distance the deflection sensitivity must be calculated to add to the piezo position. To achieve this, 25 force curves were collected over a 2.5 × 2.5 μm area on acetone cleaned silicon wafers. The deflection sensitivity can then be calculated using the gradient of the "constant compliance" region of the obtained force-curves. Using Hooke's law, the force acting on the cantilever can be calculated by multiplying the deflection and spring constant together, and force-distance curves could be plotted.

For non-printed control ppHex coated substrates, 100 force-curves were recorded for each of three 10 × 10 μm areas, using a triplicate of each colloidal probe particle type prepared.

For TPP printed surfaces, a pattern was produced with varying ridge spacings which was positioned so the ridges were perpendicular to the traverse direction of the colloidal probe. Force-curves were then collected using the three colloidal probe types on 1 μm and 3 μm high

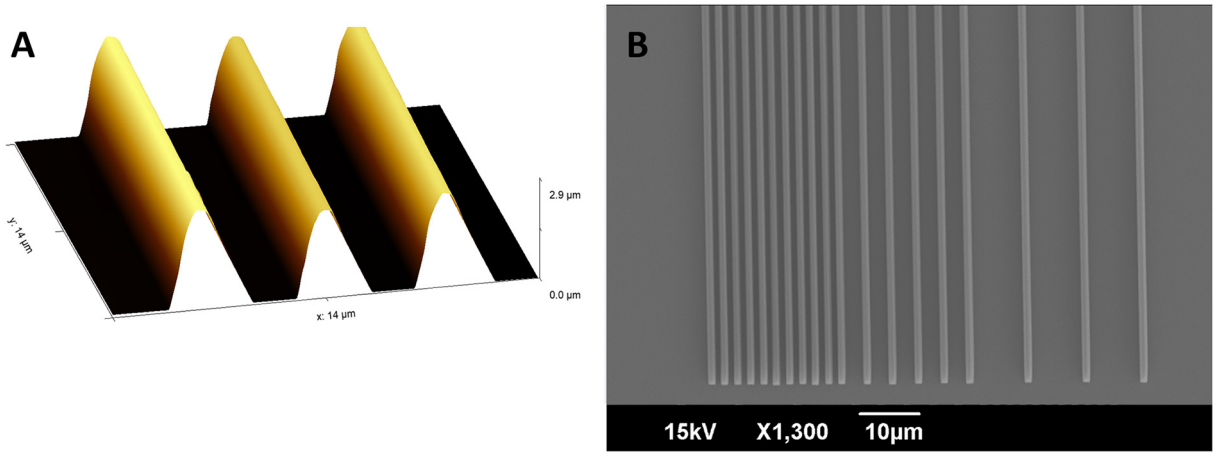

Fig. 2. A series of Two Photon Polymerised 3 μm high ridges shown by A) AFM as a 3D representation, demonstrating the height measurement and B) SEM, demonstrating the "barcode" pattern with varying spacing used for force mapping.

Table 1
Particle Adhesion to non-printed ppHex coated surfaces, and the particle adhesion normalised by particle contact area.

Particle	Adhesion (nN)	Normalised adhesion for contact area ($nN/\mu m^2$)
Polystyrene 10 μm bead	995 ± 228	0.16
Polystyrene 5 μm bead	570 ± 49	0.13
Respitose SV003 particle	409 ± 59	0.56

ridges. There was an inability to collect force maps on the 5 μm high ridges, when using the small polystyrene bead, owing to the cantilever losing surface contact. An area of 60 μm by 10 μm was evaluated, with measurements recorded every 200 nm on the X axis and every micron on the Y axis, producing a total of 3000 force-curves per scan area. Post scan, the coverage of all three spacings was established and if misaligned a second scan was undertaken to ensure a sufficient data set of each combination, all force-curves from both scans were analysed and included in the analysis. All the adhesion measurements on each

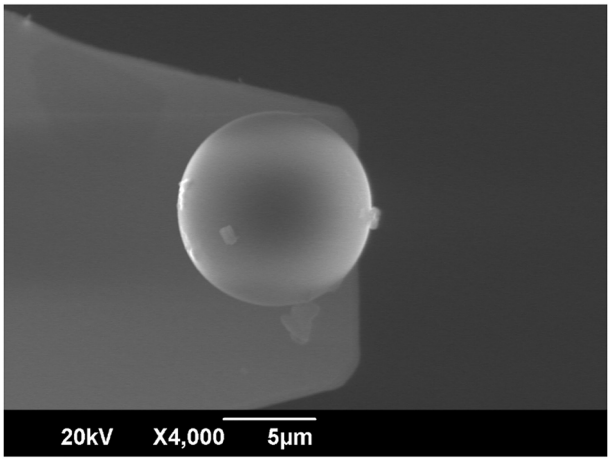

Fig. 5. SEM image of a polystyrene 10 μm bead used for force-volume mapping, showing an asperity on the tip surface.

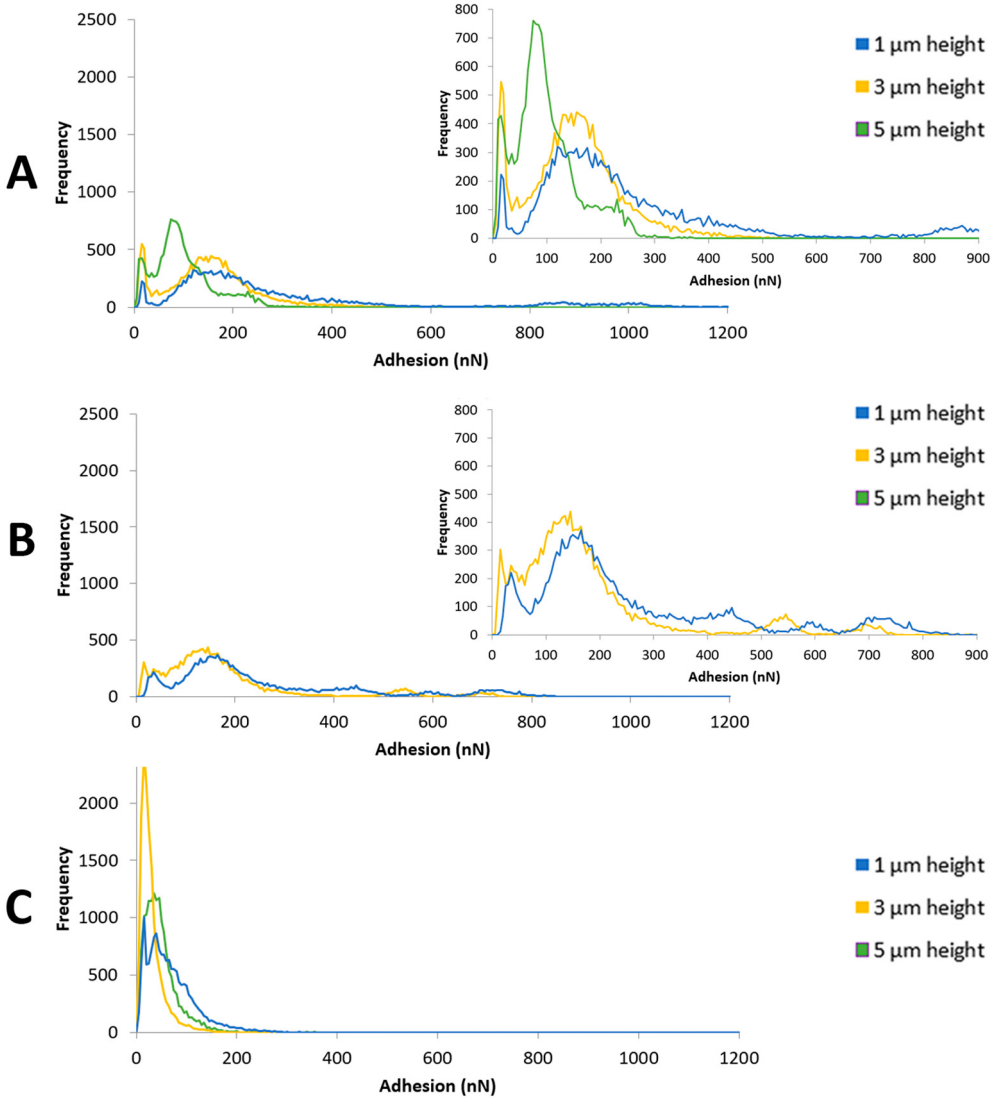

Fig. 4. Frequency curves displaying the force of adhesion calculated from the force-curves collected with all particles of each type. Each curve is normalised to total count. Adhesion to 1 μm (blue), 3 μm (yellow) and 5 μm (green) ridge heights for A) polystyrene 10 μm beads, B) polystyrene 5 μm beads and C) Respitose SV003 particles is displayed. Inset shown for A and B with focusing on the 0–900 nN data region.

TPP printed pattern were repeated in triplicate for each particle probe to ensure repeatability and account for any individual particle asperities. To ensure no damage or morphological changes occurred to the particle during the adhesion measurements, which would invalidate the results, particle probes were examined before and after each force curve scan using a tip characterisation grating (TGT1, Moscow, Russia) to image the contacting asperities of the particle [39].

Force-curves were then processed using an in-house macro, produced by Dr. Xinyong Chen to calculate the force of adhesion from the cantilever displacement. This software evaluates each force curve collected and calculates the maximum adhesion force as the difference between the cantilever free level and the trough of any discrepancy between the traces of the descent and retraction trace (See Section 3, Supplementary information).

Forces of adhesion to TPP printed substrates were not normalised for particle contact area, as this is likely to change based on the position of the imaging particle on the ridge and the number of ridges contacting with the particle, affecting the degree of particle-surface contact. This is particularly problematic with the Respitose SV003 particles, which possessed multiple surface asperities of different levels of surface roughness (Supplementary Information, Fig. 3).

To gain a greater insight into how the adhesion varied over the defined morphologies; topographical images and their respective adhesion maps were plotted for each scan, using Origin 2017 (OriginLab, Massachusetts).

3. Results and discussion

3.1. Characterisation of fabricated surfaces

To effectively decouple the effects of morphology and surface energy on particulate adhesion, surfaces with well-defined geometries on the micron scale are required. A range of semi-circular ridges were printed, with a length of 50 μm and width set to 1 μm. Due to the nature of two photon polymerisation these structures can be bespoke designed, so three ridge heights were fabricated; 1 μm, 3 μm and 5 μm which was verified by AFM (Fig. 2A). The ridge height of the patterns used for force mapping was confirmed to be 0.9 μm, 2.93 μm and 5.2 μm respectively. All ridges of a given height showed similar profiles with good surface definition and so these were deemed acceptable for testing particle adhesion.

Ridges of each height were then printed in a "barcode" pattern, encompassing three sections of differing inter-ridge spacing of 1 μm, 3 μm and 8 μm (Fig. 2B). Optical Profilometry was used to confirm inter-ridge spacing. This spacing was confirmed to be within 0.1 μm using the measurement marker tool software available with the ZDot profilometer.

3.2. Particle adhesion measurements to non-printed surfaces

Force -volume mapping was conducted in three areas on ppHex coated non-printed substrates with all particle types. All 900 force-curves collected for each particle type and calculated forces of adhesion were then included in the analysis.

Fig. 3 shows that the mean forces of adhesion (± s.d.) were 995 ± 228 nN, 570 ± 49 nN, and 409 ± 59 nN for the polystyrene 10 μm bead, polystyrene 5 μm bead and the Respitose SV003 particle respectively. By evaluating the images obtained from the tip characterisation grating for each probe (particle), the contact areas at 0.5 nm were determined, using a method previously reported in our group [29]. As Table 1 shows when the adhesion force was normalised for contact area, the average force of adhesion per μm^2 for the three particles was; 0.16 nN, 0.13 nN and 0.56 nN for the polystyrene 10 μm, polystyrene 5 μm and Respitose SV003 respectively.

Due to the consistent chemistry and materials involved, when the force of adhesion to the substrate is normalised for contact area, the adhesion is very similar for the two polystyrene beads, which is to be expected. However, the Respitose SV003 particle exhibits more than three times the normalised particle adhesion, this can be explained by various factors. Firstly, as Respitose SV003 is a lactose particle, it possesses a more hydrophilic surface, and so a higher surface free energy [40], which will result in higher forces of adhesion per unit area, compared to the hydrophobic polystyrene beads. Also, surface protrusions present on the particle may deform slightly during the press on stage of the force mapping, resulting in an increase in effective contact area [39], and hence particle adhesion.

3.3. Particle adhesion measurements to printed surfaces

For all three particle types, particle adhesion was calculated for each ridge height from a series of force-maps, aligned to include the three different spacings. Fig. 4 shows the resultant forces of adhesion from all force curves and their repeats, normalised to total count. Due to difficulties of contact continuity with the surface, the results of polystyrene 5 μm beads for the 5 μm high ridges was excluded. A reduction in force of adhesion to all the printed surface morphologies compared to the non-printed surfaces was observed. However, for the polystyrene beads, the forces of adhesion measured have a wider spread with a series of peaks.

To investigate this further, the topography and respective adhesion map were plotted for each data set, Fig. 6 and Fig. 7 shows an example of each of the three particle types interaction to 1 μm high ridges. This

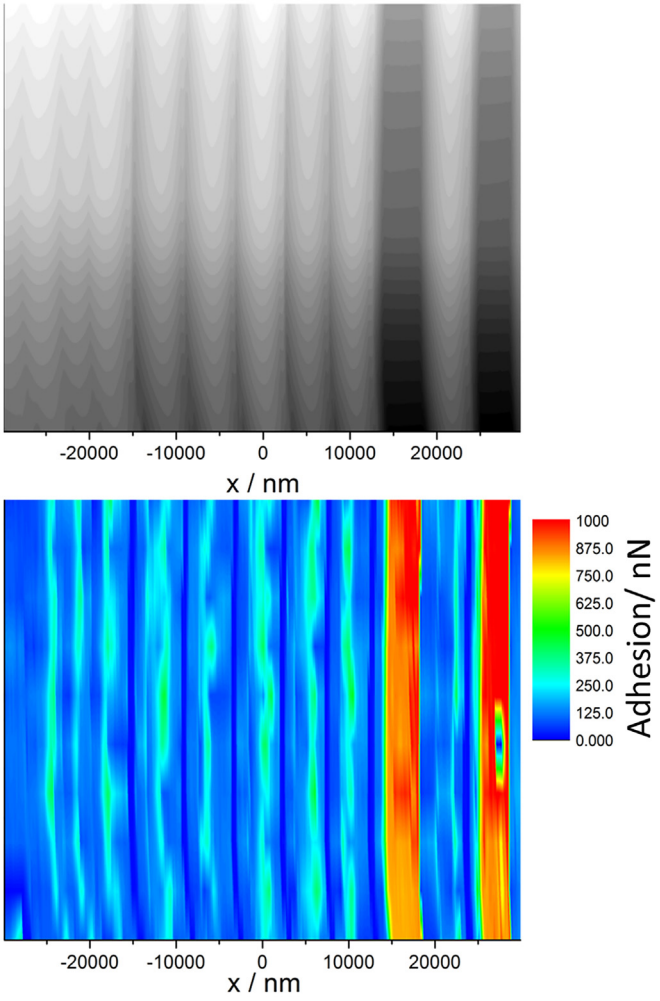

Fig. 6. Force-Volume Maps collected with CPM of a series of 1 μm high ridges with all ridge spacings, showing the topography (top) and respective adhesion (bottom) collected over the scan area with a polystyrene 10 μm bead.

clearly shows some differences between the forces of adhesion of the three particle types to the same set of ridges. Initially, for the polystyrene beads, a peak in adhesion around 1000 nN and 650 nN for the 10 μm and 5 μm bead respectively, can be seen in the 8 μm spacing between the ridges. This is likely due to the particle being in complete contact with the substrate, demonstrating similar forces of adhesion to the non-printed forces of adhesion. This similarity shows the successful isolation of the effect of morphology on the particle adhesion measurements.

For the polystyrene 10 μm bead there is a localised area of low adhesion in this region, for this particle measurement. On evaluating the SEM for this particular bead, this was shown to be likely due to a small asperity on the bead's surface (Fig. 5), resulting, we propose, in a reduction in surface contact. This localised area was absent for the other polystyrene 10 μm beads.

However, the Respitose SV003 shows no such high force of adhesion peak. As a larger particle (~ 50 μm by 30 μm) it was unable to penetrate between the ridges and contact the substrate, which is confirmed by the lack of corresponding drop in sample height in these areas on the AFM topography map.

For the polystyrene 10 μm bead, the forces of adhesion to the ridges show three adhesion intensity peaks (Fig. 4A). On the adhesion map, Fig. 6, these can be seen as dark blue, light blue and turquoise vertical lines. The dark blue low adhesion regions are aligned on the right side or in the gap between ridges, especially those of 3 μm spacing. A second adhesion region (light blue) of around 125–200 nN corresponds with an interaction with the ridges and then a slightly higher adhesion seen in turquoise, with an adhesion of around 250–300 nN, which seems to occur off-centre on the ridges. The pattern of the turquoise higher adhesion region is less consistent and shows a reduction in intensity for the polystyrene 5 μm bead in Fig. 7A and is almost completely missing for the corresponding Respitose SV003 particle adhesion map (Fig. 7B), which is consistent with the overall frequency curves seen in Fig. 4.

3.3.1. Particle adhesion measurements to printed surfaces – effect of ridge height

As an overall data set in image form, it is difficult to highlight and evaluate trends to identify how surface morphologies affect particle adhesion. Therefore, a plot was done of the average adhesion force for each ridge height – particle combination. To isolate the effect of ridge height, force of adhesion data was excluded from the 8 μm spaced ridge region of the barcode pattern. This is because for this section of the results, higher forces of adhesion were recorded when the particle was able to contact the substrate. This data would therefore skew an analysis on

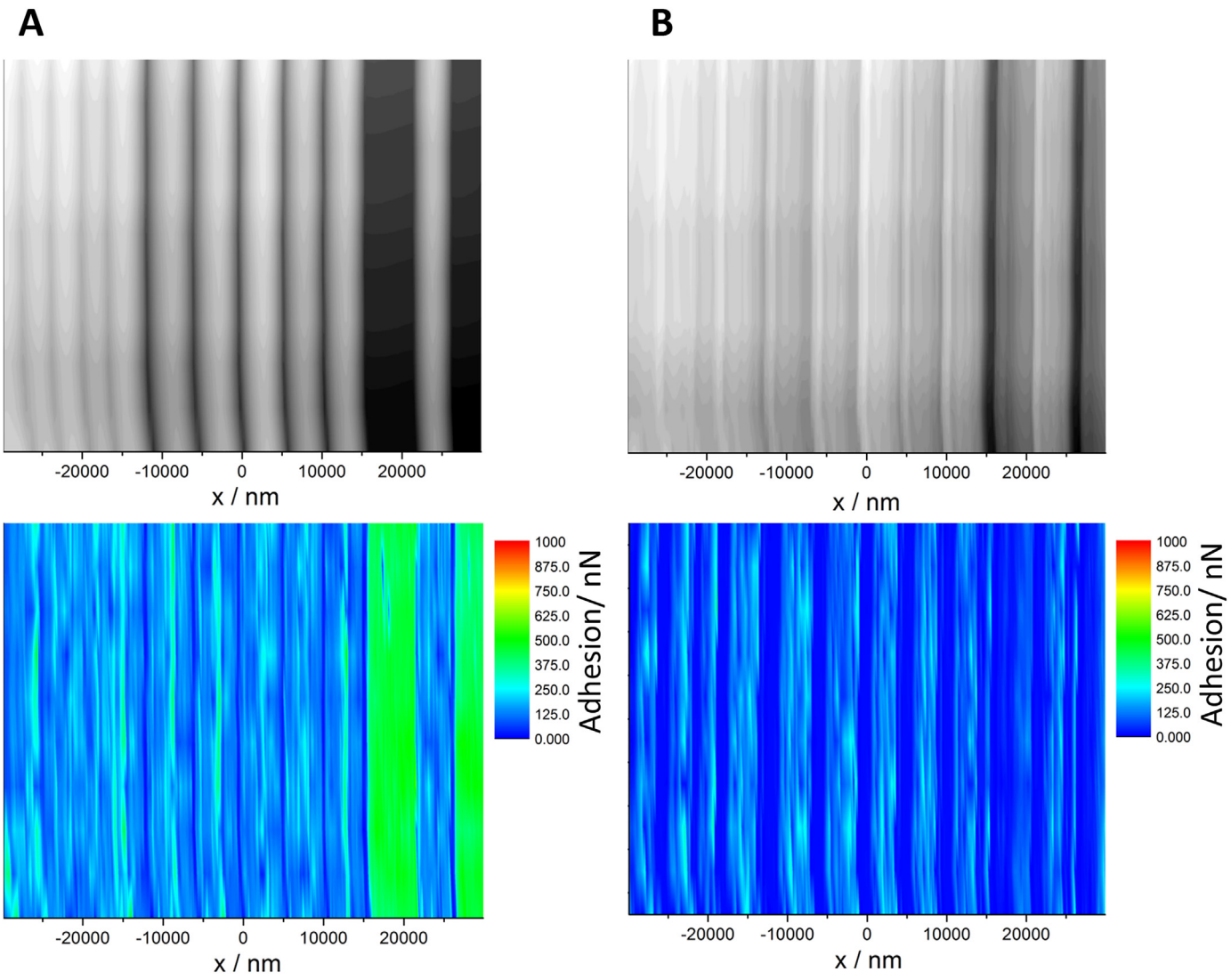

Fig. 7. Force-Volume Maps collected with CPM of a series of 1 μm high ridges with all ridge spacings, showing the topography (top) and respective adhesion (bottom) collected over the scan area with a A) polystyrene 5 μm bead and B) Respitose SV003 particle.

the effect of ridge height. As the surface chemistry has been controlled to be consistent between all the surfaces, such an approach allows direct examination of the effect of local topography and contact geometry.

As can be seen in Fig. 8, there is a clear trend of decreasing particle adhesion with increasing ridge height for both sizes of polystyrene beads. This is seen to be a significant difference for all three ridge heights, for both ridge spacings and for both polystyrene bead sizes ($p < 0.0001$).

When considering the initial ridge CAD design, the width was kept consistent for all three ridge heights, however due to the voxel nature of TPP, the top of the ridge is rounded. As a consistent width base was used with three different heights this creates a differing aspect ratio. Therefore, the rounded ridge top, will possess a smaller radius of curvature with increasing ridge height (Fig. 9). When the polystyrene beads are unable to penetrate the gaps, this means there is a reduction in effective contact area with the ridge tops as seen in Fig. 9, which is likely to be the reason for the difference in particle adhesion. To verify this, further structures of differing heights, with identical aspect ratio should be assessed.

For the Respitose SV003 particle, however this trend of decreasing particle adhesion with increasing ridge height was absent. One possible explanation could be due to asperities on the particle surface able to

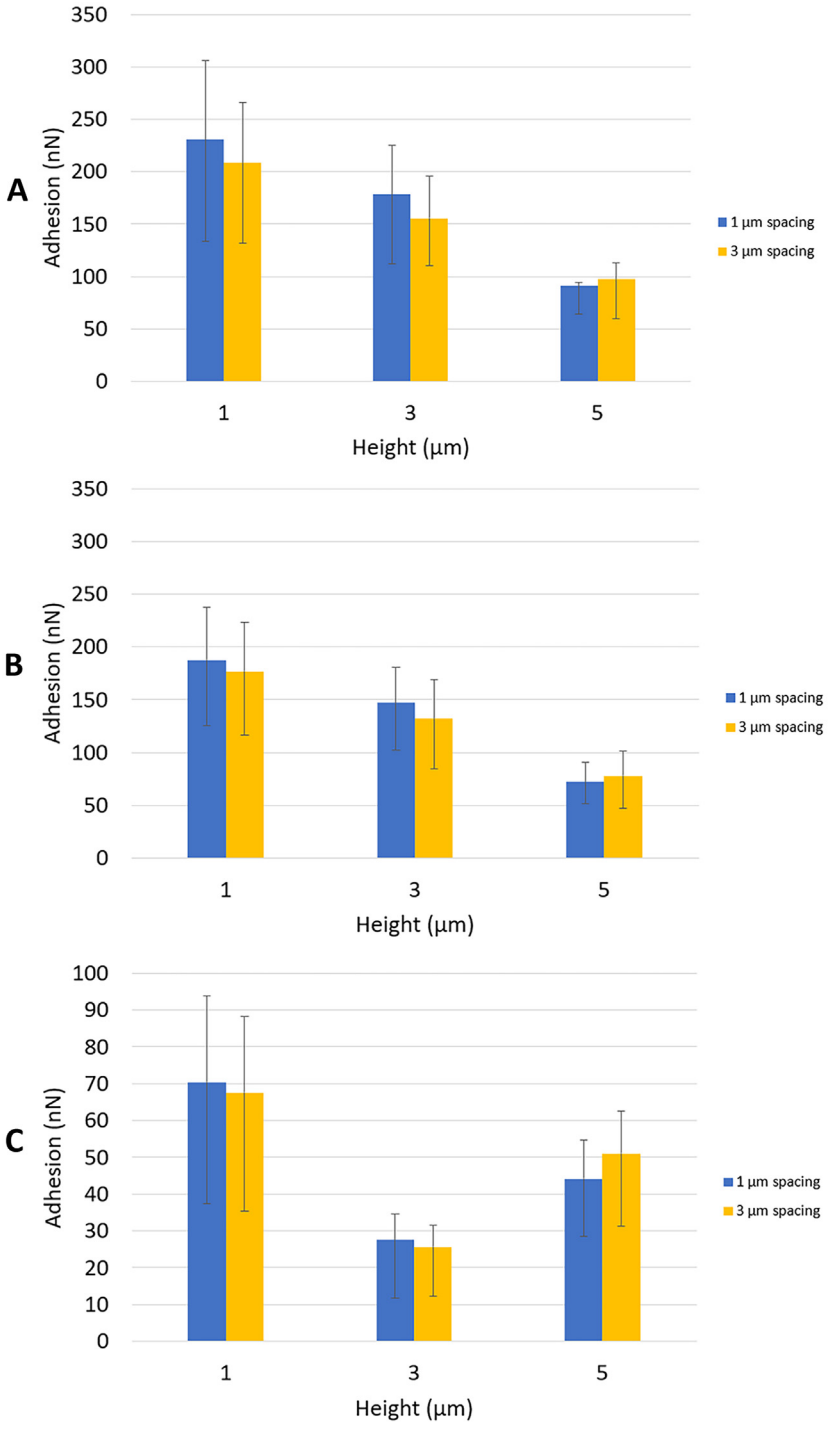

Fig. 8. An overview of the mean force of adhesion (± interquartile range), to evaluate the effect of changing ridge height for 1 µm and 3 µm ridge spacing against A) polystyrene 10 µm beads, B) polystyrene 5 µm beads, C) Respitose SV003 particles.

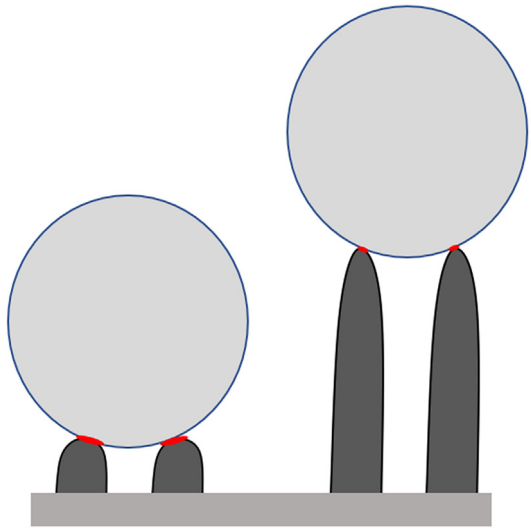

Fig. 9. A schematic representation of a 5 μm polystyrene bead interaction with 1 μm (left) and 5 μm (right) high ridges, with 1 μm spacing. This drawing is to scale and the contact area between the particle and the ridges is shown in red. (For interpretation of the references to colour in this figure legend, the reader is referred to the web version of this article.)

penetrate between the ridges and therefore contact the substrate at lower ridge heights. As the ridge height is increased the asperities or particle surface may be able to interact with the sides of the ridges differently. However, it is difficult to isolate out exactly which asperities would be in contact with which part of the ridge from the data set, ruling out a conclusive explanation. Clearly with particles of irregular shape such as Respitose, a variety of complex contact geometries is possible. The approach presented here provides a basis for these to be studied further in a controlled manner.

3.3.2. Particle adhesion measurements to printed surfaces – effect of ridge spacing

In order to assess the effect of ridge spacing, the results were evaluated for the 1 μm and 5 μm ridge heights. This is to avoid the results being biased based on whether there is a discrepancy between the two polystyrene bead sizes being able to contact the substrate (polystyrene 5 μm bead able to contact the substrate in 3 μm spacing for 3 μm ridge height, whereas polystyrene 10 μm will not). For the purposes of this analysis, the results focus on the polystyrene beads due to their ability to descend between the ridges. These results are plotted in Fig. 10.

When evaluating these results, it is difficult to see a clear trend. When the geometry allows the bead to penetrate the ridges and contact the substrate (8 μm spacing), there is a clear increase in adhesion ($p < 0.0001$). However, for the other spacings, two different trends

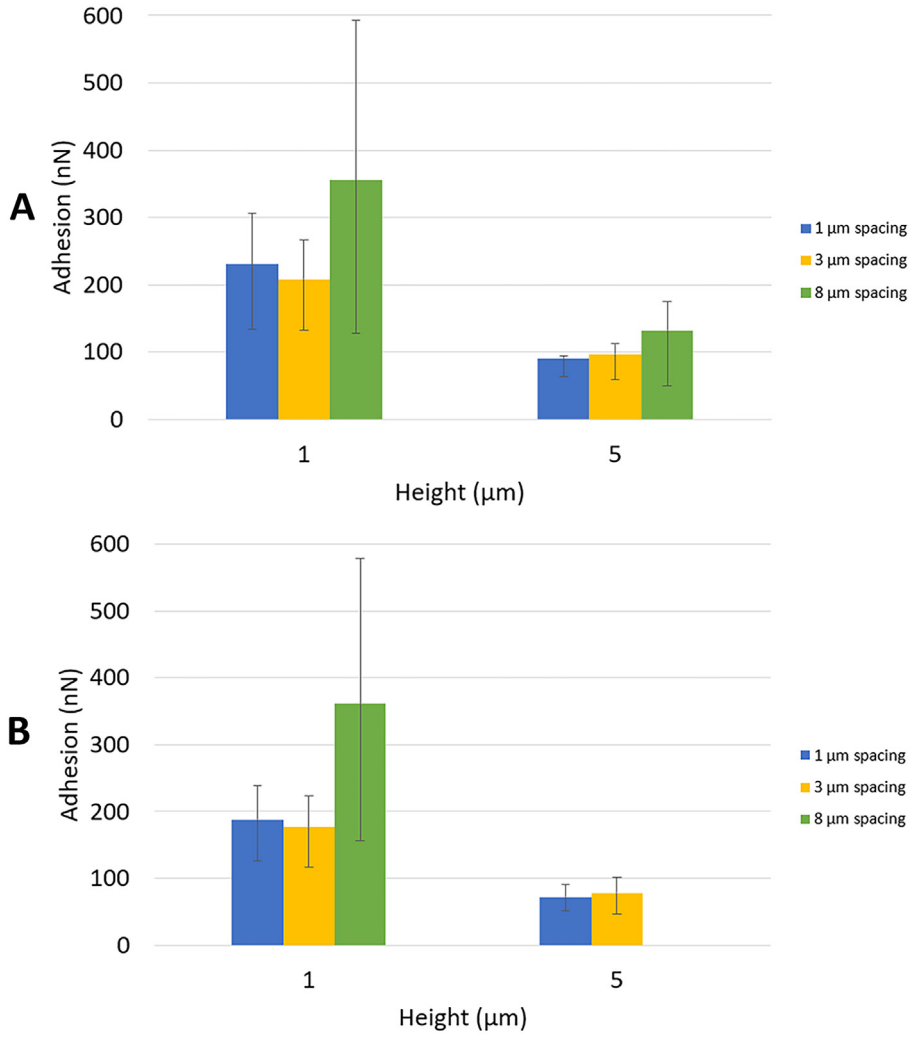

Fig. 10. An overview of the mean force of adhesion (± interquartile range), to evaluate the effect of changing ridge spacing for 1 μm and 5 μm ridge heights against A) polystyrene 10 μm beads and B) polystyrene 5 μm beads.

are seen, depending on ridge height. For 1 μm high ridges, there is a significant decrease in mean adhesion between 1 μm and 3 μm spacing, $p = 0.0004$ and 0.0481 for the polystyrene 10 μm and 5 μm beads respectively. However, the adhesion shows the opposite trend for the 5 μm high ridges, with a non-significant increase between the 1 μm and 3 μm spacings for the polystyrene 10 μm bead ($p = 0.0714$) and significant increase for the polystyrene 5 μm bead ($p = 0.0060$).

It is difficult to hypothesise a reason for this difference in trends due to multiple contributing factors. Firstly, both bead sizes will be unable to contact the substrate for the 1 μm and 3 μm spacing, but a portion of the polystyrene bead can descend into the spacing. For the 3 μm spacing a greater proportion of the sides of the beads will be available for contact with the ridges, this means an increase in adhesion would be expected. However, as mentioned earlier the curvature at the top of the ridges differs depending on ridge height, adjusting the available ridge contact area. Therefore, the sum difference in bead-ridge contact area may vary, resulting in the differing adhesion trends.

4. Conclusions

In conclusion, this paper has demonstrated the ability to produce well-defined micron scale morphologies, with varying dimensions and constant surface chemistry, of an appropriate size for particle adhesion testing. By utilising AFM force-volume mapping, the capability to elucidate the reasons behind particle-surface interaction changes has been demonstrated. Crucially, by having a map of adhesion forces, the localised fluctuation of adhesion can be investigated in detail, allowing conclusions about which aspect of a surface roughness feature is likely to be causing adhesion issues or potential solutions. This should provide significant insight allowing an optimised surface feature to be selected based on particles known to adhere. TPP can then provide the fundamental fabrication control to generate these bespoke designs.

For the initial test structures used here, the micron scale morphologies are shown to significantly reduce particle-surface adhesion compared to the flat reference substrate. Increasing ridge height is seen to significantly reduce polystyrene bead adhesion but shows no clear pattern for the irregularly shaped Respitose SV003 lactose particle. However, varying the ridge spacing produced two differing trends in adhesion to the polystyrene beads.

It would be interesting to explore the effect of particle and surface aspect ratio to confirm the likely causes of the particle-surface relationships seen. To further investigate the effect of spacing, it would be interesting to also explore a larger variety of ridge spacings. Currently this work has focused on the production of parallel ridges, and hence limited possible contact zones in a traverse direction. A logical progression, however, would be to print cross-hatch patterns allowing the interrogation of the effect of numerous contact zones from multiple directions. Finally, it would then be useful to explore different types of surface roughness to understand how the interparticulate interaction changes over different structures.

Declaration of Competing Interest

None.

Acknowledgements

AstraZeneca and the EPSRC (EP/L01646X) for funding is gratefully acknowledged. Many thanks also to Prof. Xinyong Chen (School of Pharmacy, Nottingham) for his help with AFM, and to Prof. Phil Williams (School of Pharmacy, Nottingham) with his assistance plotting the Origin figures.

Appendix A. Supplementary data

Supplementary data to this article can be found online at https://doi.org/10.1016/j.powtec.2022.117418.

References

[1] P.G.C. Petean, M.L. Aguiar, Determining the adhesion force between particles and rough surfaces, Powder Technol. 274 (2015) 67–76, https://doi.org/10.1016/j.powtec.2014.12.047.
[2] S. Peillon, A. Autricque, M. Redolfi, C. Stancu, F. Gensdarmes, C. Grisolia, O. Pluchery, Adhesion of tungsten particles on rough tungsten surfaces using atomic force microscopy, J. Aerosol Sci. 137 (2019), 105431, https://doi.org/10.1016/j.jaerosci.2019.105431.
[3] B. Laarabi, O. May Tzuc, D. Dahlioui, A. Bassam, M. Flota-Bañuelos, A. Barhdadi, Artificial neural network modeling and sensitivity analysis for soiling effects on photovoltaic panels in Morocco, Superlattice. Microst. 127 (2019) 139–150, https://doi.org/10.1016/j.spmi.2017.12.037.
[4] M. Bunker, J. Zhang, R. Blanchard, C.J. Roberts, Characterising the surface adhesive behavior of tablet tooling components by atomic force microscopy, Drug Dev. Ind. Pharm. 37 (2011) 875–885, https://doi.org/10.3109/03639045.2010.546402.
[5] M. Capece, K.R. Silva, D. Sunkara, J. Strong, P. Gao, On the relationship of inter-particle cohesiveness and bulk powder behavior: Flowability of pharmaceutical powders, Int. J. Pharm. 511 (2016) 178–189, https://doi.org/10.1016/j.ijpharm.2016.06.059.
[6] A.J. Hickey, Fundamentals of dry powder inhaler technology, Part. Nanoparticles Pharm. Prod, Springer Verlag 2018, pp. 213–232, https://doi.org/10.1007/978-3-319-94174-5_5.
[7] P. Rogliani, L. Calzetta, A. Coppola, F. Cavalli, J. Ora, E. Puxeddu, M.G. Matera, M. Cazzola, Optimizing drug delivery in COPD: the role of inhaler devices, Respir. Med. 124 (2017) 6–14, https://doi.org/10.1016/j.rmed.2017.01.006.
[8] B.K. Padhi, M.B. Chougule, A. Misra, Aerosol performance of large respirable particles of amikacin sulfate produced by spray and freeze drying techniques, Curr. Drug Deliv. 6 (2009) 8–16.
[9] S. Sarkar, B. Minatovicz, K. Thalberg, B. Chaudhuri, Development of a rational design space for optimizing mixing conditions for formation of adhesive mixtures for dry-powder inhaler formulations, J. Pharm. Sci. 106 (2017) 129–139, https://doi.org/10.1016/j.xphs.2016.07.012.
[10] M. Ariane, M. Sommerfeld, A. Alexiadis, Wall collision and drug-carrier detachment in dry powder inhalers : using DEM to devise a sub-scale model for CFD calculations, Powder Technol. 334 (2018) 65–75, https://doi.org/10.1016/j.powtec.2018.04.051.
[11] I. Sibum, P. Hagedoorn, A.H. de Boer, H.W. Frijlink, F. Grasmeijer, Challenges for pulmonary delivery of high powder doses, Int. J. Pharm. 548 (2018) 325–336, https://doi.org/10.1016/j.ijpharm.2018.07.008.
[12] A.H.L. Chow, H.H.Y. Tong, P. Chattopadhyay, B.Y. Shekunov, Particle engineering for pulmonary drug delivery, Pharm. Res. 24 (2007) 411–437, https://doi.org/10.1007/s11095-006-9174-3.
[13] D. Heng, S.H. Lee, W.K. Ng, H.-K. Chan, J.W. Kwek, R.B.H. Tan, Novel alternatives to reduce powder retention in the dry powder inhaler during aerosolization, Int. J. Pharm. 452 (2013) 194–200, https://doi.org/10.1016/j.ijpharm.2013.05.006.
[14] T. Peng, S. Lin, B. Niu, X. Wang, Y. Huang, X. Zhang, G. Li, X. Pan, C. Wu, In Fluence of Physical Properties of Carrier on the Performance of Dry Powder Inhalers, vol. 6, 2016 308–318, https://doi.org/10.1016/2016.03.011.
[15] S.C. Strathmann, M.A. Murphy, B.A. Goeckner, P.W. Carter, J.B.D. Green, Forces between insulin microspheres and polymers surfaces for a dry powder inhaler, Int. J. Pharm. 372 (2009) 147–153, https://doi.org/10.1016/j.ijpharm.2009.01.004.
[16] L.J. Jallo, Y. Chen, J. Bowen, F. Etzler, R. Dave, Prediction of inter-particle adhesion force from surface energy and surface roughness, J. Adhes. Sci. Technol. 25 (2011) 367–384, https://doi.org/10.1163/016942410X525623.
[17] R.A. Bowling, An analysis of particle adhesion on semiconductor surfaces, J. Electrochem. Soc. 132 (1985) 2208, https://doi.org/10.1149/1.2114320.
[18] S. Zellnitz, H. Schroettner, N.A. Urbanetz, Influence of surface characteristics of modified glass beads as model carriers in dry powder inhalers (DPIs) on the aerosolization performance, Drug Dev. Ind. Pharm. 00 (2015) 1–8, https://doi.org/10.3109/03639045.2014.997246.
[19] D.M. Zuev, A.K. Nguyen, V.I. Putlyaev, R.J. Narayan, 3D printing and bioprinting using multiphoton lithography, Bioprinting (2020) 30017–30018, https://doi.org/10.1016/j.bprint.2020.e00090.
[20] A. Spangenberg, N. Hobeika, F. Stehlin, J. Pierre Malval, F. Wieder, P. Prabhakaran, P. Baldeck, O. Sopper, Recent advances in two-photon stereolithography, in: S. Hosaka (Ed.), Updat. Adv. Lithogr, InTech 2013, pp. 35–63, https://doi.org/10.5772/56165.
[21] C. Liao, A. Wuethrich, M. Trau, A material odyssey for 3D nano/microstructures: two photon polymerization based nanolithography in bioapplications, Appl. Mater. Today 19 (2020), 100635, https://doi.org/10.1016/j.apmt.2020.100635.
[22] S. Maddox, M. Afshar-Mohajer, M. Zou, Digitization, replication, and modification of physical surfaces using two-photon lithography, J. Manuf. Process. 54 (2020) 180–189, https://doi.org/10.1016/j.jmapro.2020.02.042.
[23] S. Kawata, H.B. Sun, T. Tanaka, K. Takada, Finer features for functional microdevices, Nature 412 (2001) 697–698, https://doi.org/10.1038/35089130.
[24] G.R. Salazar-Banda, M.A. Felicetti, J.A.S. Gonçalves, J.R. Coury, M.L. Aguiar, Determination of the adhesion force between particles and a flat surface, using the centrifuge technique, Powder Technol. 173 (2007) 107–117, https://doi.org/10.1016/j.powtec.2006.12.011.
[25] J. Knoll, W.R. Dammert, H. Nirschl, Integration of a microscope into a centrifuge for adhesion force measurement of particles, Powder Technol. 305 (2017) 147–155, https://doi.org/10.1016/j.powtec.2016.09.065.
[26] U. Zafar, C. Hare, A. Hassanpour, M. Ghadiri, Drop test: a new method to measure the particle adhesion force, Powder Technol. 264 (2014) 236–241, https://doi.org/10.1016/j.powtec.2014.04.022.
[27] S. Ripperger, K. Hein, Measurement of adhesion forces in air with the vibration method, China Particuol. (2005) https://doi.org/10.1016/s1672-2515(07)60152-3.

[28] L. Cheong, W. Zhao, S. Song, C. Shen, Lab on a tip : applications of functional atomic force microscopy for the study of electrical properties in biology, Acta Biomater. 99 (2019) 33–52, https://doi.org/10.1016/j.actbio.2019.08.023.

[29] J.C. Hooton, C.S. German, S. Allen, M.C. Davies, C.J. Roberts, S.J. Tendler, P. Williams, Characterization of particle-interactions by atomic force microscopy: effect of contact area, Pharm. Res. 20 (2003) 508–514, https://doi.org/10.1023/A:1022684911383.

[30] C. Weiss, P. McLoughlin, H. Cathcart, Characterisation of dry powder inhaler formulations using atomic force microscopy, Int. J. Pharm. 494 (2015) 393–407, https://doi.org/10.1016/j.ijpharm.2015.08.051.

[31] M. Kappl, H.-J. Butt, The colloidal probe technique and its application to adhesion force measurements, Part. Part. Syst. Charact. 19 (2002) 129–143, https://doi.org/10.1002/1521-4117(200207)19:3<129::AID-PPSC129>3.0.CO;2-G.

[32] C.J. Roberts, What can we learn from atomic force microscopy adhesion measurements with single drug particles? Eur. J. Pharm. Sci. 24 (2005) 153–157, https://doi.org/10.1016/j.ejps.2004.11.002.

[33] N. Islam, R.A. Tuli, G.A. George, T.R. Dargaville, Colloidal drug probe: method development and validation for adhesion force measurement using atomic force microscopy, Adv. Powder Technol. 25 (2014) 1240–1248, https://doi.org/10.1016/j.apt.2014.06.021.

[34] M. Krieg, G. Fläschner, D. Alsteens, B.M. Gaub, W.H. Roos, G.J.L. Wuite, H.E. Gaub, C. Gerber, Y.F. Dufrêne, D.J. Müller, Atomic force microscopy-based mechanobiology, Nat. Rev. Phys. (2019) https://doi.org/10.1038/s42254-018-0001-7.

[35] D. Hegemann, Plasma polymerization and its application in textiles, Indian J. Fibre Text. Res. 31 (2006) 99–115.

[36] H.J. Griesser, Small scale reactor for plasma processing of moving substrate web, Vacuum. 39 (1989) 485–488, https://doi.org/10.1016/0042-207X(89)90272-8.

[37] M. Zelzer, D. Albutt, M.R. Alexander, N.A. Russell, The role of albumin and fibronectin in the adhesion of fibroblasts to plasma polymer surfaces, Plasma Process. Polym. 9 (2012) 149–156, https://doi.org/10.1002/ppap.201100054.

[38] J.L. Hutter, J. Bechhoefer, Calibration of atomic-force microscope tips, Rev. Sci. Instrum. 64 (1993) 1868–1873, https://doi.org/10.1063/1.1143970.

[39] J.C. Hooton, C.S. German, S. Allen, M.C. Davies, C.J. Roberts, S.J.B. Tendler, P.M. Williams, An atomic force microscopy study of the effect of nanoscale contact geometry and surface chemistry on the adhesion of pharmaceutical particles, Pharm. Res. 21 (2004) 953–961, https://doi.org/10.1023/B:PHAM.0000029283.47643.9c.

[40] Z. Arsoy, B. Ersoy, A. Evcin, M.G. Icduygu, Influence of dry grinding on physicochemical and surface properties of talc, Physicochem. Probl. Miner. Process. 53 (2017) 288–306, https://doi.org/10.5277/ppmp170124.